ACS APPLIED MATERIALS & INTERFACES

Research Article

www.acsami.org

Hydrotalcite-like $Ni(OH)_2$ Nanosheets in Situ Grown on Nickel Foam for Overall Water Splitting

Yuan Rao, Yang Wang, Hui Ning, Peng Li, and Mingbo Wu*

State Key Laboratory of Heavy Oil Processing, College of Chemical Engineering, China University of Petroleum, Qingdao 266580, China

Supporting Information

ABSTRACT: Designing economical and high-efficiency electrocatalysts for overall water splitting is urgently needed but remains a long and arduous task. Herein, we synthesized hydrotalcite-like $Ni(OH)_2$ nanosheets growing on Ni foam ($Ni(OH)_2$/NF) via a facile one-pot hydrothermal method. With the assistance of a rotating oven, $Ni(OH)_2$ nanosheets demonstrate a regular hexagonal morphology and homogeneous distribution. The resultant $Ni(OH)_2$/NF electrode shows superior electrocatalytic activity and durability for the hydrogen evolution reaction (HER) and oxygen evolution reaction (OER), as well as the overall water splitting. The $Ni(OH)_2$/NF electrode delivers 20 mA·cm^{-2} at an overpotential of 172 mV for HER, 50 mA·cm^{-2} at an overpotential of 330 mV for OER, and 10 mA·cm^{-2} at a cell voltage of 1.68 V for water electrolysis in 1.0 M KOH. The present study demonstrates a feasible and effective strategy to prepare highly efficient electrocatalysts for water electrolysis.

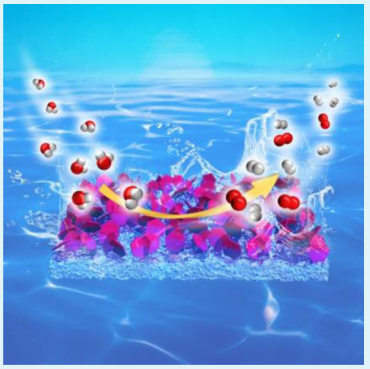

KEYWORDS: *$Ni(OH)_2$, nickel foam, hydrogen evolution reaction, oxygen evolution reaction, overall water splitting*

INTRODUCTION

Strong dependence on fossil fuels has aroused concern due to their aggravation of globe warming and pollution. Thus, searching for clean, renewable energy alternatives is an imminent need. Electrochemical water splitting is a reliable technology for storing and transporting peak excess electricity from wind and solar energy, which can realize theoretical zero pollution by producing hydrogen and oxygen merely.[1] Currently, the two reactions involved in water splitting still require high overpotentials to obtain decent reaction rates. Pt-based materials[2] and Ir/Ru-based oxides[3] remain the most efficient electrocatalysts for hydrogen evolution reaction (HER) and oxygen evolution reaction (OER), respectively. However, these noble metals suffer from scarcity and high cost, as well as instability, limiting their widespread application. So far, many earth-abundant catalysts with high activities for HER (chalcogenides,[3−11] phosphides,[5,12−17] carbides,[18−22] and nitrides[23,24]) and OER (cobalt phosphate,[5,25] oxides[26−29] and hydroxides[30−39]) have been designed. Nevertheless, it is still difficult to couple two electrocatalysts in a single electrolyzer for water electrolysis, since their optimal working conditions usually differ from each other.[43] Therefore, it is extremely advisible to design efficient non-noble electrocatalysts which show good compatibility for both HER and OER simultaneously.

Nickel is a metal with higher abundance and lower price among the six main non-noble metals (W, Mo, Co, Cu, Ni, and Fe) used in constructing HER or OER electrocatalysts.[1] Particularly, as a 3D porous foam metal with superior conductivity, Ni foam has been used in many self-supported electrodes for overall water splitting, including NiSe/Ni foam,[40] Ni_3S_2/Ni foam,[41] NiFe LDH/Ni foam,[42] MoO_x/Ni_3S_2/Ni foam,[43] Ni_2P/Ni/Ni foam,[44] and NiS/Ni foam.[45]

$Ni(OH)_2$/Ni foam has shown excellent electrochemical activities for Li-ion batteries[46] and supercapacitors,[47,48] confirming its superior conductivity and stability in alkaline electrolytes. Moreover, transition metal (hydro)oxides are considered that have a remarkable effect on cleaving the HO−H bond, in which $Ni(OH)_2$ is leading the pack, while these materials exhibit a poor ability to convert the resulting reactive hydrogen intermediates (H_{ad}) into H_2.[49−51] Conversely, transition metals including Ni are not efficient in the prior step of water dissociation but good at adsorbing and recombining the H_{ad}.[50] Hence, optimal electrocatalysts for overall water splitting can be designed by establishing novel bifunctional metal (hydro)oxides−metal systems (metal (hydro)oxides loaded on metal substrates), such as Ni-$(OH)_2$/Ni foam. However, to our best knowledge, only one publication reported $Ni(OH)_2$/Ni foam requiring corrosion in NaCl aqueous solution utilized for water splitting,[52] which gives an irregular morphology and unremarkable performance on electrocatalysis.

Herein we develop a facile method similar to a previously reported strategy[46] to in situ grow $Ni(OH)_2$ nanosheets on Ni foam via hydrothermal treatment in pure water. $Ni(OH)_2$

Received: September 1, 2016
Accepted: November 18, 2016
Published: December 5, 2016

DOI: 10.1021/acsami.6b11023
ACS Appl. Mater. Interfaces 2016, 8, 33601−33607

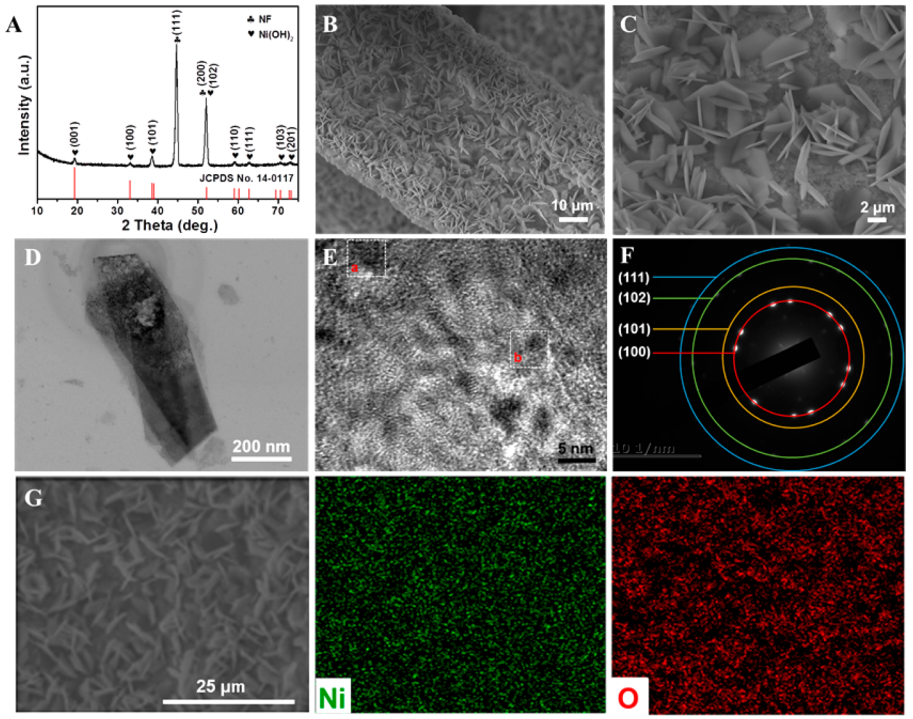

Figure 1. (A) XRD pattern of $Ni(OH)_2$/NF. (B) Low- and (C) high-magnification SEM images of $Ni(OH)_2$/NF. (D) STEM and (E) HRTEM images (see more details in Figure S5) and (F) SAED pattern taken from $Ni(OH)_2$ nanosheets. (G) EDX elemental mapping of Ni and O for $Ni(OH)_2$/NF.

nanosheets with regular hexagonal morphology can be homogeneously distributed on Ni foam.

EXPERIMENTAL SECTION

Ni foam was purchased from Suzhou Jia Shi De Foam Metal Co. Ltd. Pt/C (20 wt %), Nafion (5 wt %), and RuO_2 were purchased from Sigma-Aldrich Chemical Reagent Co. Ltd. The water used in the overall experiments was purified by a Millipore system.

Synthesis of $Ni(OH)_2$/NF. To remove the surface nickel oxides, Ni foam (1 cm × 4 cm) was ultrasonically cleaned by acetone and HCl solution (3 M) for 15 min in turn and subsequently rinsed with water and ethanol for three times.[43] The cleaned Ni foam was immersed into 50 mL of deionized water in a Teflon-lined stainless autoclave (60 mL), then sealed, and kept rotating at 160 °C for 24 h. The resultant sample was washed with ethanol three times and dried at 60 °C for 2 h. The weight increment (x mg) of Ni Foam can be directly calculated after the growth of $Ni(OH)_2$. $Ni(OH)_2$ loading = (x mg) × ($M_{Ni(OH)_2}/2M_{OH}$) = (x mg) × (93/34) = 2.7x mg, where M stands for the atomic or molecular weight. For as-prepared $Ni(OH)_2$/NF electrode, the loading mass of $Ni(OH)_2$ is about 2.9 mg·cm^{-2}.

Characterization and Instrumentations. The XRD patterns of the materials were recorded on a PANalytical X-ray diffractometer (Cu Kα radiation, k = 0.15406 nm, 40 kV, 40 mA). XPS spectrum was performed by ESCALAB 250XI instrument (Al Kα, hυ = 1486.6 eV). All XRD and XPS patterns were characterized by using $Ni(OH)_2$/NF materials. The Raman spectra were obtained from a Renishaw Raman system model 2000 spectrometer. SEM measurements were collected on a ZEISS MERLIN scanning electron microscope at 20 kV. STEM images were obtained from JEM2100F scanning transmission electron microscopy (JEOL, Tokyo, Japan) at 200 kV.

Electrochemical Measurements. All electrochemical measurements were carried out on a CHI 760E electrochemical analyzer (CHI Instruments, Inc., Shanghai) in a standard three-electrode system, during which $Ni(OH)_2$/NF (0.8 cm × 0.8 cm) was utilized as the working electrode, while a carbon rod as the counter electrode and an Ag/AgCl electrode as the reference electrode in 1.0 M KOH solution. All potentials shown in this study were calibrated to RHE by the following equation: E(RHE) = E(Ag/AgCl) + (0.197 V) + 0.059pH.[40] The linear sweep voltammetry (LSV) was tested from 0 to 0.6 V at a scan rate of 5 mV/s without any activation process before recording the polarization curves, and the LSV curves were not corrected by iR correction. When the current density was calculated, the working surface area was calculated by a single side.[40−45] The durabilities of the resultant materials were tested by chronoamperometric measurements. For comparative purposes, the 20 wt % Pt/C and RuO_2 loaded electrodes were prepared with the same loading amount and working surface area as $Ni(OH)_2$/NF according to a previously reported method.[43] In a typical procedure, (1) 6 mg of Pt/C or RuO_2 and 10 μL 5 wt % Nafion solution were dispersed in 800 μL of ethanol by 60 min sonication to acquire a homogeneous mixture, (2) 250 μL of this solution was pipetted onto Ni foam to ensure the compared electrode has the same working area of $Ni(OH)_2$/NF (0.64 cm^{-2}) and a certain loading amount of 2.9 mg·cm^{-2}, and (3) 80 μL of 0.5 wt % Nafion solution dissolved in ethanol was drop-cast on the surface of the electrode to prevent the covering materials from falling off and then left to dry in air.

Evaluation of Electrochemically Active Surface Area. Based on reported methods,[44] electrochemically active surface areas (ECSAs) can be estimated from the electrochemical double layer capacitance (C_{dl}) through collecting cyclic voltammograms (CVs) in a non-Faradaic region due to ECSA being proportional to the C_{dl} value in the same material. C_{dl} of resultant materials were derived from a sequence of CV tests with different scan rates (10, 20, 40, 60, 80, and 100 mV·s^{-1}) in the potential range from 0.1 to 0.2 V versus RHE. Through a plot of different scan rates versus the corresponding current density (j) between the anode and cathode ($j_{anodic} - j_{cathodic}$) at 0.15 V versus RHE, a linear slope was calculated as C_{dl}.[43]

RESULTS AND DISCUSSION

Following by direct hydrothermal treatment in pure water, the Ni foam substrate turns into black (see the Supporting Information, Figure S1). The XRD pattern of $Ni(OH)_2$/NF is shown in Figure 1A; the two peaks at 44.5 and 51.8° arise from Ni (JCPDS No. 65-2865). Diffraction peaks apart from

DOI: 10.1021/acsami.6b11023
ACS Appl. Mater. Interfaces 2016, 8, 33601−33607

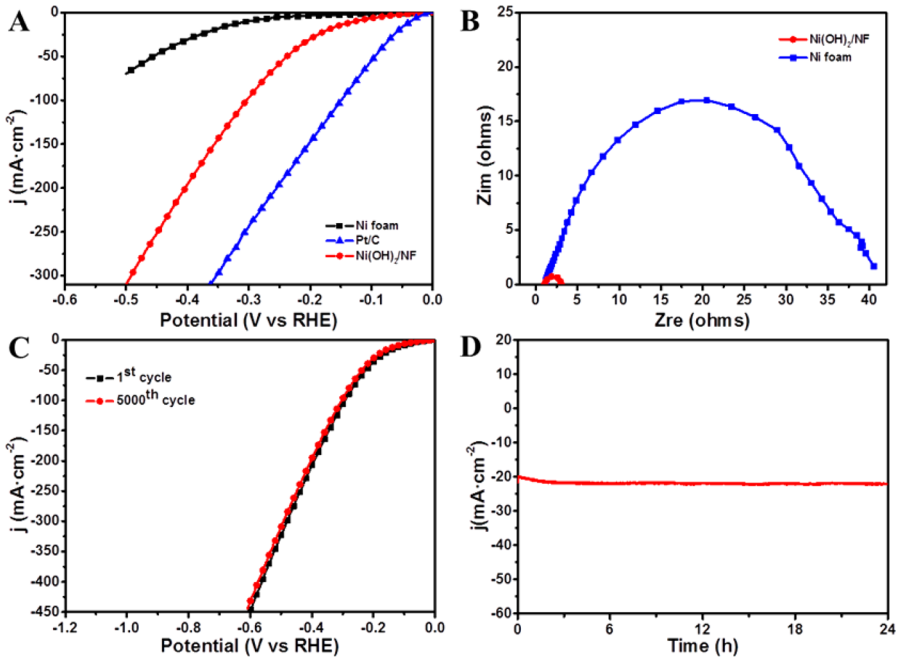

Figure 2. (A) LSV curves for $Ni(OH)_2$/NF, Pt/C, and bare Ni foam without *iR* correction at a sweep rate of 5 mV/s. (B) Nyquist plots of $Ni(OH)_2$/NF and the bare Ni foam measured at an overpotential of −200 mV. (C) LSV curves for $Ni(OH)_2$/NF before and after 5000 cycles between 0 and −0.6 V. (D) Chronoamperometric curve of $Ni(OH)_2$/NF at an overpotential of 172 mV for 24 h.

those of Ni correspond to (001), (100), (101), (102), (110), (111), (103), and (201) planes of hexagonal β-$Ni(OH)_2$ (JCPDS No. 14-0117).[46] The formation of $Ni(OH)_2$ was further confirmed by Raman spectroscopy (Figure S2). The X-ray photoelectron spectroscopy (XPS) analysis of $Ni(OH)_2$/NF indicates the characteristic peaks of Ni and O (Figure S3A), and the C 1s signal is due to CO_2 in the testing atmosphere. Ni $2p_{1/2}$ and Ni $2p_{3/2}$ centered at 873.0 and 855.4 eV correspond to Ni^{II} (Figure S3B). The O 1s peak intensity is relatively strong which indicates a significant oxidation on the surface and the formation of $Ni(OH)_2$ (Figure S3C). The formation of β-$Ni(OH)_2$ can be ascribed to the weak oxidation reaction of Ni in pure water:[46]

$$Ni + nH_2O \rightarrow [Ni(H_2O)_n]^{2+} + 2e^- \quad (1)$$

$$O_2 + 2H_2O + 4e^- \rightarrow 4OH^- \quad (2)$$

$$[Ni(H_2O)_n]^{2+} + 2OH^- \rightarrow Ni(OH)_2 + nH_2O \quad (3)$$

As displayed in the low-magnification SEM image of $Ni(OH)_2$/NF (Figure 1B), the surface of Ni foam substrate was completely covered by $Ni(OH)_2$ nanosheets, and the 3D macroporous morphology remains similar to that of the pristine nickel foam (Figure S4). Figure 1G shows the corresponding elemental mapping images of Ni and O of $Ni(OH)_2$/NF which demonstrate that Ni and O elements evenly distribute in the $Ni(OH)_2$ nanosheets. The high-magnification SEM image (Figure 1C) further reveals that $Ni(OH)_2$ nanosheets grow vertically over Ni foam and spatially interconnect, forming a typical hydrotalcite-like structure. These $Ni(OH)_2$ nanosheets show an average size about 4 μm with a thickness of dozens of nanometers. The high-resolution TEM (HRTEM) images derived from $Ni(OH)_2$ nanosheets (Figures 1E and S5) display well-distinguishable lattice fringes with interplanar distances of 1.56 and 4.60 Å (Figure S5) indexed to the (110) and (001) planes of β-$Ni(OH)_2$, respectively. The related selected area electron diffraction (SAED) pattern (Figure 1F) exhibits discrete spots indexed to the (111), (102), (101), and (100) planes of β-$Ni(OH)_2$ phase. All these observations strongly support the successful growth of $Ni(OH)_2$ nanosheets on Ni foam merely after one-step hydrothermal treatment in pure water.

The electrocatalytic activity of $Ni(OH)_2$/NF for HER was investigated in a typical three-electrode system using $Ni(OH)_2$/NF as the working electrode directly. For comparison, bare Ni foam and 20 wt % Pt/C coated on Ni foam with the same loading mass of $Ni(OH)_2$/NF were also tested.[43,45] The $Ni(OH)_2$/NF electrode demonstrates excellent electrocatalytic performance toward HER (Figure 2A), affording a current density of 10, 20, 50, 100, and 300 $mA{\cdot}cm^{-2}$ without *iR* correction at overpotentials of 127, 172, 237, 303, and 492 mV, respectively. Compared to the typical Co- or Ni-based bifunctional catalysts, $Ni(OH)_2$/NF exhibits a lower overpotential (Table S1). The Tafel slope can be calculated from the plot based on the Tafel equation ($\eta = a + b \log j$, where η is the overpotential, j is the current density, and b is the Tafel slope),[45] which is 56, 140, and 206 $mV{\cdot}dec^{-1}$ for Pt/C, $Ni(OH)_2$/NF, and the bare Ni foam, respectively (Figure S6). The much higher HER activity of $Ni(OH)_2$/NF compared to that of bare Ni foam can also be supported by its smaller semicircular diameter in the electric impedance spectrum (Figure 2B), implying smaller contact resistance and charge transfer impedance of $Ni(OH)_2$/NF. The durability of the electrode was evaluated by comparing the LSV curves of as-prepared $Ni(OH)_2$/NF before and after 5000 cycles (Figure 2C); the material gives almost the same onset potential and current density, representing a superior long-term durability. Furthermore, the chronoamperometric measurement of Ni-$(OH)_2$/NF indicates that $Ni(OH)_2$/NF retains its catalytic activity even after 24 h electrocatalytic testing (Figure 2D). Its microstructure and morphology remain intact, as proved in the

DOI: 10.1021/acsami.6b11023
ACS Appl. Mater. Interfaces 2016, 8, 33601−33607

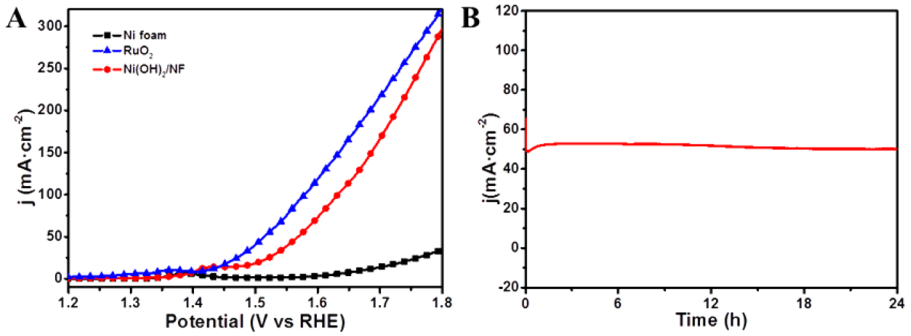

Figure 3. (A) LSV curves for $Ni(OH)_2$/NF, RuO_2, and bare Ni foam without *iR* correction at a sweep rate of 5 mV/s. (B) Chronoamperometric curve of $Ni(OH)_2$/NF at an overpotential of 330 mV over 24 h.

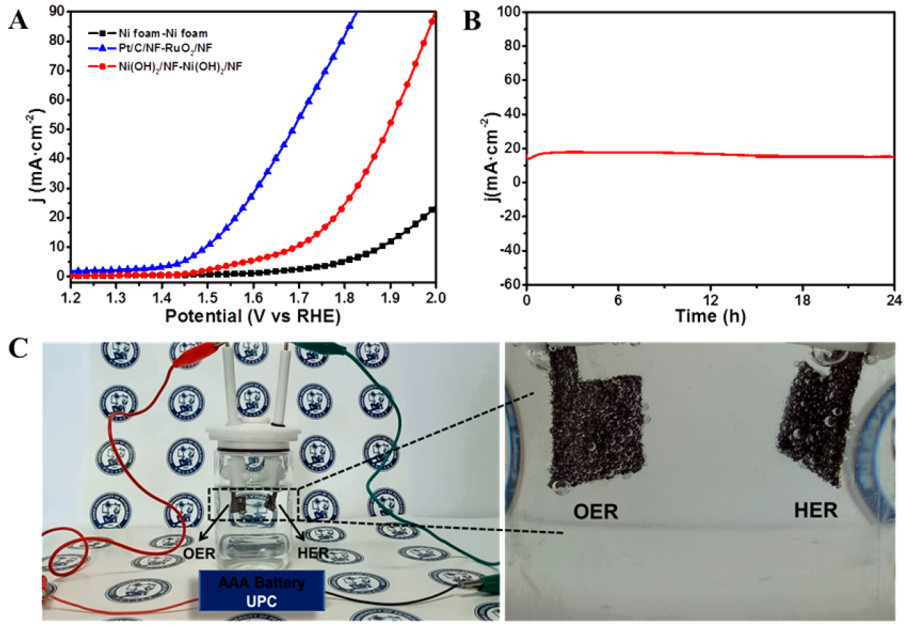

Figure 4. (A) LSV curves of an electrolyzer containing a $Ni(OH)_2$/NF-$Ni(OH)_2$/NF, Pt/C-RuO_2 or Ni foam-Ni foam couple for overall water splitting without *iR* correction at a scan rate of 5 mV/s. (B) Chronoamperometric curve of water electrolysis for $Ni(OH)_2$/NF in a two-electrode configuration at a static potential of 1.75 V. (C) Digital photographs of the electrolyzer driven by one AAA battery (1.5 V) with $Ni(OH)_2$/NF applied as both anode and cathode. Logo used with permission from China University of Petroleum.

XRD pattern (Figure S7A), SEM image (Figure S7B), and XPS spectra (Figure S3B,C).

The catalytic properties of $Ni(OH)_2$/NF for OER were also investigated in 1.0 M KOH and compared with the bare Ni foam and RuO_2 loaded on Ni foam. As shown in Figure 3A, the $Ni(OH)_2$/NF electrode exhibits much higher catalytic activity for OER than bare Ni foam and slightly lower catalytic activity than RuO_2 on Ni foam. The oxidation peak at 1.43 V versus RHE of $Ni(OH)_2$/NF is ascribed to the transformation of Ni^{II} to Ni^{III}.[53] The widely recognized surface Faradaic reaction of nickel hydroxide[54] is as follow:

$$Ni(OH)_2 + OH^- \rightarrow NiOOH + H_2O + e^-$$

$Ni(OH)_2$/NF can afford a current density of 10, 20, 50, 100, and 200 $mA{\cdot}cm^{-2}$ without *iR* correction at overpotentials of 170, 270, 330, 400, and 490 mV, respectively (Figure 3A), which prevails over the behaviors of most reported Ni- or Co-based OER or bifunctional catalysts (Table S1). The Tafel slopes of RuO_2, $Ni(OH)_2$/NF, and the bare Ni foam are 124, 150, and 194 $mV{\cdot}dec^{-1}$, respectively (Figure S8). The long-term electrochemical stability of $Ni(OH)_2$/NF electrode was probed in 1.0 M KOH (Figure 3B), and it can stabilize around 50 $mA{\cdot}cm^{-2}$ at a static potential of about 1.56 V during the 24 h testing. $Ni(OH)_2$/NF can mainly retain initial morphology and microstructure after long-time electrocatalytic OER (Figure S9B). And its phase compositions also remain nearly unchanged, as evident from its XRD pattern (Figure S9A) and XPS spectra (Figure S3B,C).

Given that $Ni(OH)_2$/NF had remarkable electrocatalytic property toward both HER and OER in 1 M KOH, with the satisfying free-standing bifunctional electrode, we constructed an electrolyzer with a two-electrode system utilizing $Ni(OH)_2$/NF as both anode and cathode for water electrolysis. The electrolyzer delivers a current density of 10 $mA{\cdot}cm^{-2}$ at 1.68 V without *iR* correction (Figure 4A). Despite this value being inferior to that of Pt/C/Ni foam||RuO_2/Ni foam (1.50 V), it outperforms state-of-the-art electrolyzers utilizing Co- or Ni-based bifunctional electrorcatalysts for overall water splitting (Table S1). Furthermore, the long-term stability of this system was also tested; when the static potential of 1.75 V was applied, the electrolyzer afforded a constant current density around 15 $mA{\cdot}cm^{-2}$ for at least 24 h without obvious decay (Figure 4B).

DOI: 10.1021/acsami.6b11023
ACS Appl. Mater. Interfaces 2016, 8, 33601−33607

Meanwhile, the electrolyzer can be driven by one AAA battery with 1.5 V (Figure 4C).

Interestingly, the rotating assistance is found to be significant for forming a uniform morphology of $Ni(OH)_2$/NF. $Ni(OH)_2$ nanosheets with a regular hexagonal morphology and homogeneous distribution (Figure 1B) can be obtained via rotating assistance, while $Ni(OH)_2$ nanosheets with disorder morphology and unevenly distributed are observed without rotating (Figures S10 and S11). The $Ni(OH)_2$/NF synthesized with no rotary assistance (denoted $Ni(OH)_2$/NF-2) displays inferior HER and OER performance (Figure S12A,B). In addition, the reaction time also plays a major role in the formation of $Ni(OH)_2$/NF, a series of reaction times (12, 18, 24, 36, and 48 h) were investigated, and 24 h is found to be the preferable reaction time to give superior electrocatalytic activities among the investigated values (Figure S13A,B). When the reaction time was halved, i.e., 12 h, while keeping the other reaction parameters unchanged, $Ni(OH)_2$ nanosheets did not form on the Ni foam (Figure S14A,B). On the other hand, when the reaction time was increased to 48 h, a rapid increase was found in the thickness of $Ni(OH)_2$ nanosheets (Figure S15A,B).

Based on results discussed above, the excellent electrocatalytic performance of $Ni(OH)_2$/NF for both HER and OER reactions can be ascribed to the following four factors: (i) The oxygen in water initiates the self-growth of ultrathin $Ni(OH)_2$ on Ni foam that enables strong mechanical adhesion and fast charge transfer pathways without any polymer binder, facilitating the elimination of the interfacial overpotential between $Ni(OH)_2$ nanosheets and Ni foam. (ii) The nanosheets and hydrotalcite-like architecture of $Ni(OH)_2$/NF largely increase the active areas and accessible catalytic sites, which greatly facilitate ion and electron diffusion; this can be proved by the electrochemically active surface area (ECSA) calculation result that $Ni(OH)_2$/NF has about 118 times larger ECSA than bare Ni foam (Figure S16). (iii) There is a synergistic effect between $Ni(OH)_2$ nanosheets and Ni foam; Ni^{2+} on $Ni(OH)_2$ has plenty of unfilled d orbitals and possesses strong electrostatic affinity to OH^- generated by water dissociation, thus markedly accelerating the first step ($H_2O + e^- \rightarrow H_{ad} + OH^-$) of overall water splitting in alkaline media; then the effective adsorption and recombination of H_{ad} proceed on Ni substrate. (iv) The nanoporous architecture of electrode surface can transform the three phase contact line of gas bubbles with the solid electrode into a discontinuous state, resulting in extremely low adhesive force between them and excellent bubble departure ability, thus promoting the electrocatalytic performance of $Ni(OH)_2$/NF.[55]

CONCLUSIONS

In summary, a novel and facile strategy has been developed to prepare binder-free catalysts for water electrolysis via in situ growth of $Ni(OH)_2$ nanosheets on Ni foam. The hydrotalcite-like $Ni(OH)_2$/NF electrode possesses remarkable electrocatalytic activity and durability for both HER and OER reactions under strongly alkaline conditions. The corresponding two-electrode water electrolyzer using $Ni(OH)_2$/NF as both anode and cathode demonstrates an efficient system achieving 10 $mA \cdot cm^{-2}$ at a cell voltage of 1.68 V with superior stability. This study contributes an economical and high-efficiency method to develop a self-supported noble-metal-free electrocatalyst for overall water splitting.

ASSOCIATED CONTENT

Supporting Information

The Supporting Information is available free of charge on the ACS Publications website at DOI: 10.1021/acsami.6b11023.

Optical photographs, SEM images, HRTEM images, XRD patterns, cyclic voltammograms, Tafel plots, Raman and XPS spectra of the $Ni(OH)_2$/NF electrode, comparison of the electrocatalytic activities over $Ni(OH)_2$/NF materials obtained from different reaction conditions, and comparison of the electrocatalytic performance of $Ni(OH)_2$/NF vis-à-vis bifunctional water splitting or OER electrocatalysts reported recently (PDF)

AUTHOR INFORMATION

Corresponding Author

*E-mail: wumb@upc.edu.cn.

ORCID

Yuan Rao: 0000-0002-6770-6230

Notes

The authors declare no competing financial interest.

ACKNOWLEDGMENTS

This work was supported by the National Natural Science Foundation of China (Grant Nos. 51372028 and 51372277) and the Fundamental Research Fund for the Central Universities (Grant No. 15CX08005A).

REFERENCES

(1) Zou, X.; Zhang, Y. Noble Metal-Free Hydrogen Evolution Catalysts for Water Splitting. *Chem. Soc. Rev.* **2015**, *44*, 5148−5180.

(2) Tian, J.; Liu, Q.; Asiri, A. M.; Sun, X. Self-Supported Nanoporous Cobalt Phosphide Nanowire Arrays: An Efficient 3D Hydrogen-Evolving Cathode over the Wide Range of pH 0−14. *J. Am. Chem. Soc.* **2014**, *136*, 7587−7590.

(3) Lee, Y.; Suntivich, J.; May, K. J.; Perry, E. E.; Shao-Horn, Y. Synthesis and Activities of Rutile IrO_2 and RuO_2 Nanoparticles for Oxygen Evolution in Acid and Alkaline Solutions. *J. Phys. Chem. Lett.* **2012**, *3*, 399−404.

(4) Yu, L.; Xia, B.; Wang, X.; Lou, X. General Formation of M-MoS_3 (M = Co, Ni) Hollow Structures with Enhanced Electrocatalytic Activity for Hydrogen Evolution. *Adv. Mater.* **2016**, *28*, 92−97.

(5) Wang, J.; Cui, W.; Liu, Q.; Xing, Z.; Asiri, A. M.; Sun, X. Recent Progress in Cobalt-Based Heterogeneous Catalysts for Electrochemical Water Splitting. *Adv. Mater.* **2016**, *28*, 215−230.

(6) Zhang, L.; Wu, H.; Yan, Y.; Wang, X.; Lou, X. Hierarchical MoS_2 Microboxes Constructed by Nanosheets with Enhanced Electrochemical Properties for Lithium Storage and Water Splitting. *Energy Environ. Sci.* **2014**, *7*, 3302−3306.

(7) Chen, K.; Li, C.; Chen, Z.; Shi, L.; Reddy, S.; Meng, H.; Ji, Q.; Zhang, Y.; Liu, Z. Bioinspired Synthesis of CVD Graphene Flakes and Graphene-Supported Molybdenum Sulfide Catalysts for Hydrogen Evolution Reaction. *Nano Res.* **2016**, *9*, 249−259.

(8) Zhang, Y.; Shi, J.; Han, G.; Li, M.; Ji, Q.; Ma, D.; Zhang, Y.; Li, C.; Lang, X.; Zhang, Y.; Liu, Z. Chemical Vapor Deposition of Monolayer WS_2 Nanosheets on Au Foils toward Direct Application in Hydrogen Evolution. *Nano Res.* **2015**, *8*, 2881−2890.

(9) Jia, L.; Sun, X.; Jiang, Y.; Yu, S.; Wang, C. A Novel $MoSe_2$-Reduced Graphene Oxide/Polyimide Composite Film for Applications in Electrocatalysis and Photoelectrocatalysis Hydrogen Evolution. *Adv. Funct. Mater.* **2015**, *25*, 1814−1820.

(10) Pu, Z.; Luo, Y.; Asiri, A. M.; Sun, X. Efficient Electrochemical Water Splitting Catalyzed by Electrodeposited Nickel Diselenide

DOI: 10.1021/acsami.6b11023
ACS Appl. Mater. Interfaces 2016, 8, 33601−33607

Nanoparticles Based Film. *ACS Appl. Mater. Interfaces* **2016**, *8*, 4718−4723.
(11) Liu, T.; Asiri, A. M.; Sun, X. Electrodeposited Co-doped $NiSe_2$ Nanoparticles Film: a Good Electrocatalyst for Efficient Water Splitting. *Nanoscale* **2016**, *8*, 3911−3915.
(12) Zhou, D.; He, L.; Zhu, W.; Hou, X.; Wang, K.; Du, G.; Zheng, C.; Sun, X.; Asiri, A. M. Interconnected Urchin-like Cobalt Phosphide Microspheres Film for Highly Efficient Electrochemical Hydrogen Evolution in Both Acidic and Basic Media. *J. Mater. Chem. A* **2016**, *4*, 10114−10117.
(13) Popczun, E. J.; Read, C. G.; Roske, C. W.; Lewis, N. S.; Schaak, R. E. Highly Active Electrocatalysis of The Hydrogen Evolution Reaction by Cobalt Phosphide Nanoparticles. *Angew. Chem., Int. Ed.* **2014**, *53*, 5427−5430.
(14) Jiang, P.; Liu, Q.; Liang, Y.; Tian, J.; Asiri, A. M.; Sun, X. A Cost-Effective 3D Hydrogen Evolution Cathode with High Catalytic Activity: FeP Nanowire Array as the Active Phase. *Angew. Chem.* **2014**, *126*, 13069−13073.
(15) Tian, J.; Liu, Q.; Cheng, N.; Asiri, A. M.; Sun, X. Self-Supported Cu_3P Nanowire Arrays as an Integrated High-Performance Three-Dimensional Cathode for Generating Hydrogen from Water. *Angew. Chem., Int. Ed.* **2014**, *53*, 9577−9581.
(16) Zhu, W.; Tang, C.; Liu, D.; Wang, J.; Asiri, A. M.; Sun, X. A Self-Standing Nanoporous MoP_2 Nanosheet Array: an Advanced pH-Universal Catalytic Electrode for the Hydrogen Evolution Reaction. *J. Mater. Chem. A* **2016**, *4*, 7169−7173.
(17) Yang, H.; Zhang, Y.; Hu, F.; Wang, Q. Urchin-like CoP Nanocrystals as Hydrogen Evolution Reaction and Oxygen Reduction Reaction Dual-Electrocatalyst with Superior Stability. *Nano Lett.* **2015**, *15*, 7616−7620.
(18) Youn, D. H.; Han, S.; Kim, J. Y.; Kim, J. Y.; Park, H.; Choi, S. H.; Lee, J. S. Highly Active and Stable Hydrogen Evolution Electrocatalysts Based on Molybdenum Compounds on Carbon Nanotube-Graphene Hybrid Support. *ACS Nano* **2014**, *8*, 5164−5173.
(19) Chen, W.-F.; Wang, C.-H.; Sasaki, K.; Marinkovic, N.; Xu, W.; Muckerman, J.; Zhu, Y.; Adzic, R. Highly Active and Durable Nanostructured Molybdenum Carbide Electrocatalysts for Hydrogen Production. *Energy Environ. Sci.* **2013**, *6*, 943−951.
(20) Chen, W.-F.; Muckerman, J. T.; Fujita, E. Recent Developments in Transition Metal Carbides and Nitrides as Hydrogen Evolution Electrocatalysts. *Chem. Commun.* **2013**, *49*, 8896−8909.
(21) Ma, F.; Wu, H.; Xia, B.; Xu, C.; Lou, X. Hierarchical β-Mo_2C Nanotubes Organized by Ultrathin Nanosheets as a Highly Efficient Electrocatalyst for Hydrogen Production. *Angew. Chem., Int. Ed.* **2015**, *54*, 15395−15399.
(22) Alhajri, N. S.; Anjum, D. H.; Takanabe, K. Molybdenum Carbide-Carbon Nanocomposites Synthesized from a Reactive Template for Electrochemical Hydrogen Evolution. *J. Mater. Chem. A* **2014**, *2*, 10548−10556.
(23) Chen, W.-F.; Sasaki, K.; Ma, C.; Frenkel, A. I.; Marinkovic, N.; Muckerman, J. T.; Zhu, Y.; Adzic, R. R. Hydrogen-Evolution Catalysts Based on Non-Noble Metal Nickel-Molybdenum Nitride Nanosheets. *Angew. Chem., Int. Ed.* **2012**, *51*, 6131−6135.
(24) Cao, B.; Veith, G. M.; Neuefeind, J. C.; Adzic, R. R.; Khalifah, P. G. Mixed Close-Packed Cobalt Molybdenum Nitrides as Non-noble Metal Electrocatalysts for the Hydrogen Evolution Reaction. *J. Am. Chem. Soc.* **2013**, *135*, 19186−19192.
(25) Kanan, M. W.; Nocera, D. G. In Situ Formation of an Oxygen-Evolving Catalyst in Neutral Water Containing Phosphate and Co^{2+}. *Science* **2008**, *321*, 1072−1075.
(26) Smith, R. D. L.; Prevot, M. S.; Fagan, R. D.; Zhang, Z.; Sedach, P. A.; Siu, M. K.; Trudel, S.; Berlinguette, C. P. Photochemical Route for Accessing Amorphous Metal Oxide Materials for Water Oxidation Catalysis. *Science* **2013**, *340*, 60−63.
(27) Jung, J. I.; Jeong, H. Y.; Lee, J. S.; Kim, M. G.; Cho, J. A Bifunctional Perovskite Catalyst for Oxygen Reduction and Evolution. *Angew. Chem., Int. Ed.* **2014**, *53*, 4582−4586.
(28) Ma, T.; Dai, S.; Jaroniec, M.; Qiao, S. Metal-Organic Framework Derived Hybrid Co_3O_4-Carbon Porous Nanowire Arrays as Reversible Oxygen Evolution Electrodes. *J. Am. Chem. Soc.* **2014**, *136*, 13925−13931.
(29) Zhu, Y.; Zhou, W.; Chen, Z.; Chen, Y.; Su, C.; Tade, M. O.; Shao, Z. $SrNb_{0.1}Co_{0.7}Fe_{0.2}O_{3-\delta}$ Perovskite as a Next-Generation Electrocatalyst for Oxygen Evolution in Alkaline Solution. *Angew. Chem., Int. Ed.* **2015**, *54*, 3897−3910.
(30) Long, X.; Li, J.; Xiao, S.; Yan, K.; Wang, Z.; Chen, H.; Yang, S. A Strongly Coupled Graphene and FeNi Double Hydroxide Hybrid as an Excellent Electrocatalyst for the Oxygen Evolution Reaction. *Angew. Chem., Int. Ed.* **2014**, *53*, 7584−7588.
(31) Chemelewski, W. D.; Lee, H.-C.; Lin, J.-F.; Bard, A. J.; Mullins, C. B. Amorphous FeOOH Oxygen Evolution Reaction Catalyst for Photoelectrochemical Water Splitting. *J. Am. Chem. Soc.* **2014**, *136*, 2843−2850.
(32) Song, F.; Hu, X. Ultrathin Cobalt-Manganese Layered Double Hydroxide is an Efficient Oxygen Evolution Catalyst. *J. Am. Chem. Soc.* **2014**, *136*, 16481−16484.
(33) Trotochaud, L.; Young, S. L.; Ranney, J. K.; Boettcher, S. W. Nickel-Iron Oxyhydroxide Oxygen-Evolution Electrocatalysts: the Role of Intentional and Incidental Iron Incorporation. *J. Am. Chem. Soc.* **2014**, *136*, 6744−6753.
(34) Li, X.; Han, G.; Liu, Y.; Dong, B.; Hu, W.; Shang, X.; Chai, Y.; Liu, C. NiSe@NiOOH Core−Shell Hyacinth-like Nanostructures on Nickel Foam Synthesized by in Situ Electrochemical Oxidation as an Efficient Electrocatalyst for the Oxygen Evolution Reaction. *ACS Appl. Mater. Interfaces* **2016**, *8*, 20057−20066.
(35) Zhao, Z.; Wu, H.; He, H.; Xu, X.; Jin, Y. A High-Performance Binary Ni−Co Hydroxide-based Water Oxidation Electrode with Three-Dimensional Coaxial Nanotube Array Structure. *Adv. Funct. Mater.* **2014**, *24*, 4698−4705.
(36) Liu, P. F.; Yang, S.; Zheng, L. R.; Zhang, B.; Yang, H. G. Electrochemical Etching of α-Cobalt Hydroxide for Improvement of Oxygen Evolution Reaction. *J. Mater. Chem. A* **2016**, *4*, 9578−9584.
(37) Gao, M.; Sheng, W.; Zhuang, Z.; Fang, Q.; Gu, S.; Jiang, J.; Yan, Y. Efficient Water Oxidation Using Nanostructured α-Nickel-Hydroxide as an Electrocatalyst. *J. Am. Chem. Soc.* **2014**, *136*, 7077−7084.
(38) Yoon, T.; Kim, K. S. One-Step Synthesis of CoS-Doped β-$Co(OH)_2$@Amorphous MoS_{2+x} Hybrid Catalyst Grown on Nickel Foam for High-Performance Electrochemical Overall Water Splitting. *Adv. Funct. Mater.* **2016**, *26*, 7386−7393.
(39) Liu, Z.; Yu, C.; Han, X.; Yang, J.; Zhao, C.; Huang, H.; Qiu, J. CoMn-Layered Double Hydroxides/Carbon Nanotubes Architectures as High-Performance Electrocatalysts for Oxygen Evolution Reaction. *ChemElectroChem* **2016**, *3*, 906−912.
(40) Tang, C.; Cheng, N.; Pu, Z.; Xing, W.; Sun, X. NiSe Nanowire Film Supported on Nickel Foam: An Efficient and Stable 3D Bifunctional Electrode for Full Water Splitting. *Angew. Chem., Int. Ed.* **2015**, *54*, 9351−9355.
(41) Feng, L.; Yu, G.; Wu, Y.; Li, G.; Li, H.; Sun, Y.; Asefa, T.; Chen, W.; Zou, X. High-Index Faceted Ni_3S_2 Nanosheet Arrays as Highly Active and Ultrastable Electrocatalysts for Water Splitting. *J. Am. Chem. Soc.* **2015**, *137*, 14023−14026.
(42) Luo, J.; Im, J.-H.; Mayer, M. T.; Schreier, M.; Nazeeruddin, M. K.; Park, N.-G.; Tilley, S. D.; Fan, H. J.; Grätzel, M. Water Photolysis at 12.3% Efficiency via Perovskite Photovoltaics and Earth-abundant Catalysts. *Science* **2014**, *345*, 1593−1596.
(43) Wu, Y.; Li, G.; Liu, Y.; Yang, L.; Lian, X.; Asefa, T.; Zou, X. Overall Water Splitting Catalyzed Efficiently by an Ultrathin Nanosheet-Built, Hollow Ni_3S_2-Based Electrocatalyst. *Adv. Funct. Mater.* **2016**, *26*, 4839−4847.
(44) You, B.; Jiang, N.; Sheng, M.; Bhushan, M. W.; Sun, Y. Hierarchically Porous Urchin-Like Ni_2P Superstructures Supported on Nickel Foam as Efficient Bifunctional Electrocatalysts for Overall Water Splitting. *ACS Catal.* **2016**, *6*, 714−721.
(45) Zhu, W.; Yue, X.; Zhang, W.; Yu, S.; Zhang, Y.; Wang, J.; Wang, J. Nickel Sulfide Microsphere Film on Ni foam as an Efficient Bifunctional Electrocatalyst for Overall Water Splitting. *Chem. Commun.* **2016**, *52*, 1486−1489.

DOI: 10.1021/acsami.6b11023
ACS Appl. Mater. Interfaces 2016, 8, 33601−33607

(46) Ni, S.; Lv, X.; Li, T.; Yang, X.; Zhang, L. The Investigation of $Ni(OH)_2$/Ni as Anodes for High Performance Li-ion Batteries. *J. Mater. Chem. A* **2013**, *1*, 1544−1547.
(47) Hu, B.; Qin, X.; Asiri, A. M.; Alamry, K. A.; Al-Youbi, A. O.; Sun, X. Fabrication of $Ni(OH)_2$ Nanoflakes Array on Ni foam as a Binder-free Electrode Material for High Performance Supercapacitors. *Electrochim. Acta* **2013**, *107*, 339−342.
(48) Xiong, X.; Ding, D.; Chen, D.; Waller, G.; Bu, Y.; Wang, Z.; Liu, M. Three-Dimensional Ultrathin $Ni(OH)_2$ Nanosheets Grown on Nickel Foam for High-Performance Supercapacitors. *Nano Energy* **2015**, *11*, 154−161.
(49) Xu, Y.; Gao, M.; Zheng, Y.; Jiang, J.; Yu, S. Nickel/Nickel(II) Oxide Nanoparticles Anchored onto Cobalt(IV) Diselenide Nanobelts for the Electrochemical Production of Hydrogen. *Angew. Chem., Int. Ed.* **2013**, *52*, 8546−8550.
(50) Subbaraman, R.; Tripkovic, D.; Strmcnik, D.; Chang, K.; Uchimura, M.; Paulikas, A. P.; Stamenkovic, V.; Markovic, N. M. Enhancing Hydrogen Evolution Activity in Water Splitting by Tailoring Li^+-$Ni(OH)_2$-Pt Interfaces. *Science* **2011**, *334*, 1256−1260.
(51) Wang, L.; Lin, C.; Huang, D.; Chen, J.; Jiang, L.; Wang, M.; Chi, L.; Shi, L.; Jin, J. Optimizing the Volmer Step by Single-Layer Nickel Hydroxide Nanosheets in Hydrogen Evolution Reaction of Platinum. *ACS Catal.* **2015**, *5*, 3801−3806.
(52) Lee, J.; Lim, G.-H.; Lim, B. Nanostructuring of Metal Surface by Corrosion for Efficient Water Splitting. *Chem. Phys. Lett.* **2016**, *644*, 51−55.
(53) Louie, M. W.; Bell, A. T. An Investigation of Thin-Film Ni-Fe Oxide Catalysts for the Electrochemical Evolution of Oxygen. *J. Am. Chem. Soc.* **2013**, *135*, 12329−12337.
(54) Wang, H.; Casalongue, H. S.; Liang, Y.; Dai, H. $Ni(OH)_2$ Nanoplates Grown on Graphene as Advanced Electrochemical Pseudocapacitor Materials. *J. Am. Chem. Soc.* **2010**, *132*, 7472−7477.
(55) Lu, Z.; Zhu, W.; Yu, X.; Zhang, H.; Li, Y.; Sun, X.; Wang, X.; Wang, H.; Wang, J.; Luo, J.; Lei, X.; Jiang, L. Ultrahigh Hydrogen Evolution Performance of Under-Water "Superaerophobic" MoS_2 Nanostructured Electrodes. *Adv. Mater.* **2014**, *26*, 2683−2687.

DOI: 10.1021/acsami.6b11023
ACS Appl. Mater. Interfaces 2016, 8, 33601−33607